

## Journal of Molecular Science

www.jmolecularsci.com

ISSN:1000-9035

**Chemical Synthesis and Comprehensive Physico-Chemical  
Characterization of Magnetic Oxide Nanoparticles for Advanced  
Functional Applications**Mugale Yogesh Gopal<sup>1</sup> & Suryawanshi Venkat S.<sup>2</sup><sup>1,2</sup>Department of Chemistry, P.G. and Research Centre, Shri Chhatrapati Shivaji College,  
Omerga.

yogeshmugale1991@gmail.com

**Article Information**

Received: 20-04-2025

Revised: 18-05-2025

Accepted: 29-05-2025

Published: 20-06-2025

**Keywords***Magnetic oxide  
nanoparticles, Chemical  
synthesis, Physico-  
chemical properties,  
Superparamagnetism,  
Nanomaterials  
characterization.***ABSTRACT**

Magnetic oxide nanoparticles (MONPs) have garnered significant attention due to their unique size-dependent magnetic, structural, and surface properties, which are critical for a wide range of advanced functional applications, including biomedicine, catalysis, and data storage. This study presents a detailed investigation into the chemical synthesis and physico-chemical characterization of MONPs, focusing primarily on ferrite-based systems such as  $\text{Fe}_3\text{O}_4$  and  $\text{CoFe}_2\text{O}_4$ . The nanoparticles were synthesized via a modified co-precipitation method, allowing control over particle size and crystallinity through variation of pH, temperature, and precursor concentration. Structural analysis using X-ray diffraction (XRD) confirmed phase purity and crystallite size, while transmission electron microscopy (TEM) revealed monodispersity and morphological features. Fourier-transform infrared spectroscopy (FTIR) and X-ray photoelectron spectroscopy (XPS) were employed to elucidate surface chemistry and functional groups. Vibrating sample magnetometry (VSM) demonstrated superparamagnetic behavior for  $\text{Fe}_3\text{O}_4$  nanoparticles and enhanced coercivity in  $\text{CoFe}_2\text{O}_4$  samples, confirming their suitability for distinct applications. Additionally, thermogravimetric analysis (TGA) provided insights into thermal stability and surface modifications. The interplay between synthesis parameters and resulting physico-chemical properties is discussed in detail, highlighting the potential for tuning MONPs for specific end-uses. This comprehensive study contributes to the growing body of knowledge on magnetic oxide nanomaterials and supports the development of customizable, high-performance nanoparticles tailored for targeted applications in nanotechnology and materials science.

**©2025 The authors**

This is an Open Access article distributed under the terms of the Creative Commons Attribution (CC BY NC), which permits unrestricted use, distribution, and reproduction in any medium, as long as the original authors and source are cited. No permission is required from the authors or the publishers. (<https://creativecommons.org/licenses/by-nc/4.0/>)

**1. INTRODUCTION**

The rapid advancement of nanotechnology has revolutionized the field of materials science, offering unparalleled opportunities to design and develop novel materials with unique properties. Among the various classes of nanomaterials, magnetic oxide nanoparticles (MONPs) have garnered significant attention due to their distinctive magnetic behavior, chemical stability, and potential for functional integration in a wide range of technological and biomedical applications. These nanoparticles typically consist of transition metal oxides, such as iron oxide ( $\text{Fe}_3\text{O}_4$  or  $\gamma\text{-Fe}_2\text{O}_3$ ), cobalt oxide ( $\text{Co}_3\text{O}_4$ ), and manganese oxide ( $\text{Mn}_3\text{O}_4$ ), which exhibit superparamagnetism, high surface area-to-volume ratio, and tunable physico-chemical characteristics at the nanoscale.

The synthesis of MONPs is a critical aspect that governs their structural, morphological, and functional properties. Various chemical synthesis routes, such as co-precipitation, sol-gel, hydrothermal, solvothermal, microemulsion, and thermal decomposition methods, have been developed to produce magnetic oxide nanoparticles with controlled size, shape, crystallinity, and surface chemistry. Each method offers distinct advantages and challenges in terms of particle uniformity, phase purity, scalability, and environmental sustainability. For instance, co-precipitation is a widely used technique due to its simplicity and cost-effectiveness, while thermal decomposition provides high crystallinity and size control at the

expense of more complex processing requirements and the use of organic solvents.

Beyond synthesis, comprehensive physico-chemical characterization is essential to evaluate and understand the behavior and potential functionality of MONPs. Characterization techniques provide insights into critical parameters such as particle size distribution, surface area, crystallographic structure, magnetic properties, surface charge (zeta potential), and chemical composition. These parameters significantly influence the performance of MONPs in various applications, including magnetic resonance imaging (MRI), targeted drug delivery, magnetic hyperthermia, catalysis, environmental remediation, and data storage technologies.

Magnetic oxide nanoparticles possess unique magnetic properties due to the presence of unpaired electrons in the d-orbitals of transition metal ions. When reduced to nanoscale dimensions, these materials may exhibit superparamagnetism, a state wherein the nanoparticles behave like single magnetic domains with high magnetic susceptibility but no remanence or coercivity in the absence of an external magnetic field. This feature is particularly advantageous in biomedical applications where particle aggregation due to residual magnetization must be minimized. The magnetic behavior of MONPs is typically assessed through techniques like vibrating sample magnetometry (VSM) and superconducting quantum interference devices (SQUID), which measure parameters such as saturation magnetization, coercivity, and remanent magnetization.

The structural and morphological features of MONPs are equally important for their functional performance. X-ray diffraction

(XRD) is commonly used to determine the crystalline phase and estimate the crystallite size using Scherrer's equation. Transmission electron microscopy (TEM) and scanning electron microscopy (SEM) provide high-resolution images of particle morphology and size distribution. Fourier-transform infrared spectroscopy (FTIR), Raman spectroscopy, and X-ray photoelectron spectroscopy (XPS) help identify surface functional groups, chemical bonding, and oxidation states of metal ions, respectively. Furthermore, Brunauer–Emmett–Teller (BET) analysis is used to determine surface area and porosity, which are critical for applications involving adsorption or catalysis.

Surface modification and functionalization of MONPs further extend their usability by enhancing colloidal stability, biocompatibility, and specificity toward target molecules. Surface coatings with biocompatible polymers (e.g., polyethylene glycol, dextran, chitosan), surfactants, or silica layers are frequently employed to improve dispersion in aqueous media and reduce cytotoxicity. These coatings also provide anchor points for conjugating drugs, targeting ligands, or fluorescent markers, thereby facilitating multifunctionality in biomedical contexts. Understanding the surface chemistry through techniques like zeta potential measurement and dynamic light scattering (DLS) is crucial for optimizing particle behavior in biological and environmental systems.

The integration of MONPs into functional applications is driven by their tailored physico-chemical properties. In medicine, iron oxide nanoparticles are employed as contrast agents in MRI due to their ability to shorten T2 relaxation times, providing enhanced imaging contrast. In oncology, MONPs are used for magnetic hyperthermia, where alternating magnetic fields induce localized heating to destroy

cancer cells. Drug delivery systems utilizing MONPs can achieve controlled and targeted release by exploiting external magnetic fields, minimizing systemic side effects. In environmental science, magnetic nanoparticles are used to remove heavy metals and organic pollutants from wastewater through magnetic separation techniques.

In catalysis, MONPs serve as active catalysts or catalyst supports in redox reactions, leveraging their high surface reactivity and stability. Their magnetic properties allow for easy recovery and reuse, which is particularly beneficial in green chemistry applications. In electronics and data storage, the unique magnetic and electronic properties of MONPs contribute to the development of high-density magnetic recording media, spintronics, and magnetic sensors.

Despite their promising applications, there remain significant challenges in the synthesis and application of MONPs. Achieving monodispersity, phase purity, and consistent surface properties on a large scale remains difficult. Additionally, understanding the long-term stability, biocompatibility, and environmental fate of MONPs is essential for safe and effective application, particularly in biomedicine and environmental remediation. As a result, ongoing research is focused on optimizing synthetic methods, developing advanced characterization protocols, and designing multifunctional nanoparticles with predictable behavior under diverse operational conditions.

Chemical synthesis and comprehensive physico-chemical characterization of magnetic oxide nanoparticles are foundational to their successful deployment in advanced functional applications. A synergistic approach combining controlled synthesis, in-depth

characterization, and application-specific surface engineering is vital to harnessing the full potential of these materials. Future research efforts must aim to bridge the gap between laboratory-scale innovation and real-world implementation, ensuring that magnetic oxide nanoparticles continue to play a transformative role in modern science and technology.

### **1.Literature Survey:**

Magnetic oxide nanoparticles (MNPs) have garnered significant attention in recent decades due to their unique physicochemical properties, making them suitable for a wide range of advanced functional applications<sup>1,2</sup>. These applications span diverse fields such as nanomedicine, environmental remediation, catalysis, and energy storage<sup>3,4</sup>. The ability to control their synthesis, tailor their properties through chemical modifications, and comprehensively characterize their resulting attributes is crucial for optimizing their performance in these applications<sup>5,6</sup>. This review aims to provide a comprehensive overview of the chemical synthesis methods, advanced physicochemical characterization techniques, and the relationship between these factors and the performance of MNPs in various functional applications. The performance of MNPs in advanced functional applications is highly dependent on their physicochemical properties, which are, in turn, determined by the synthesis method and subsequent modifications. For example, the size and shape of MNPs can significantly affect their magnetic properties and their ability to be internalized by cells for drug delivery<sup>7</sup>. Similarly, the surface chemistry of MNPs plays a crucial role in their stability in biological media and their ability to be functionalized with targeting ligands<sup>8,9</sup>. Therefore, a thorough understanding of the

synthesis methods and characterization techniques is essential for designing MNPs with optimal properties for specific applications<sup>10</sup>.

Co-precipitation is a widely used and relatively simple method for synthesizing MNPs<sup>12</sup>. It involves the simultaneous precipitation of iron ions (Fe<sup>2+</sup> and Fe<sup>3+</sup>) from an aqueous solution by adding a base, such as sodium hydroxide (NaOH) or ammonium hydroxide (NH<sub>4</sub>OH)<sup>11</sup>. The size, shape, and composition of the resulting MNPs can be controlled by adjusting various parameters, including the Fe<sup>2+</sup>/Fe<sup>3+</sup> ratio, pH, temperature, ionic strength, and the presence of capping agents<sup>13</sup>. To mitigate the oxidation issue, several strategies can be employed, such as performing the reaction under an inert atmosphere (e.g., nitrogen or argon), carefully controlling the Fe<sup>2+</sup>/Fe<sup>3+</sup> ratio to 1:2, and adding reducing agents to the solution<sup>14</sup>. Thermal decomposition involves the decomposition of organometallic precursors, such as iron oleate or iron acetylacetonate, in a high-boiling-point organic solvent at elevated temperatures<sup>15</sup>. This method allows for precise control over the size, shape, and crystallinity of the MNPs by carefully selecting the precursors, solvents, and reaction conditions. Green synthesis methods offer an environmentally friendly alternative to traditional chemical synthesis techniques<sup>18</sup>. These methods utilize biological materials, such as plant extracts, bacteria, fungi, and algae, as reducing and capping agents for the synthesis of MNPs<sup>19</sup>. Despite these limitations, green synthesis is gaining increasing attention due to its environmental benefits and potential for large-scale production of MNPs<sup>21</sup>. Table 1 shows Summary of Synthesis Methods.

**Table 1. Summary of Synthesis Methods**

Synthesis Method	Advantages	Disadvantages
Co-precipitation	Simple, cost-effective, high yield	Broad size distribution, poor shape control, oxidation potential
Thermal Decomposition	High crystallinity, narrow size distribution, good shape control	Toxic solvents, high temperatures, complex purification
Hydrothermal/Solvothermal	High crystallinity, controlled size and shape, relatively low temperatures	High pressure, long reaction times, potential aggregation
Microemulsion	Narrow size distribution, good shape control, mild conditions	Low yield, difficulty in surfactant removal, limited scalability
Sol-Gel	Relatively low temperatures, good size control, high purity	Long reaction times, shrinkage during drying, difficulty in solvent removal
Green Synthesis	Environmentally friendly, cost-effective, biocompatible	Lower yield, less control over size and shape, batch-to-batch variability

Comprehensive characterization of MNPs is crucial for understanding their properties and optimizing their performance in various applications<sup>10</sup>. Several advanced characterization techniques are employed to determine the structural, morphological, and magnetic properties of MNPs.

XRD is a powerful technique for determining the crystal structure, phase composition, and crystallite size of MNPs<sup>22,23</sup>. By analyzing the diffraction pattern, the crystalline phases present in the sample can be identified, and the

average crystallite size can be estimated using the Scherrer equation<sup>22</sup>.

TEM is a high-resolution imaging technique that provides detailed information about the size, shape, morphology, and microstructure of MNPs<sup>22,23</sup>. TEM images can reveal the presence of agglomeration, the thickness of any surface coatings, and the crystallinity of the MNPs [22]. Table 2 shows Summary of Characterization Techniques.

**Table 2. Summary of Characterization Techniques**

Characterization Technique	Information Provided
XRD	Crystal structure, phase composition, crystallite size
TEM	Size, shape, morphology, microstructure, crystallinity
SEM	Surface morphology, size distribution
DLS	Hydrodynamic size, size distribution, stability
VSM	Saturation magnetization, coercivity, remanence
Mössbauer Spectroscopy	Oxidation state, magnetic ordering, local environment of iron atoms
AFM	Surface topography, mechanical properties
FTIR	Chemical functional groups on the surface
Raman Spectroscopy	Vibrational modes, identification of iron oxide phases
Zeta Potential Analysis	Surface charge, stability
TGA	Composition, amount of organic material on the surface

Coating MNPs with polymers is a common strategy to improve their stability in physiological environments and prevent aggregation<sup>9</sup>. Polymers such as polyethylene glycol (PEG), polyvinyl alcohol (PVA), and dextran are frequently used for this purpose<sup>24</sup>. The polymer coating can also provide functional groups

for further modification with targeting ligands or therapeutic agents<sup>8</sup>. MNPs are particularly promising for biomedical applications due to their biocompatibility, magnetic properties, and ease of functionalization<sup>27</sup>. In magnetic hyperthermia, the heating efficiency of MNPs is dependent on several factors,

including size, shape, magnetic anisotropy, and the applied magnetic field. MNPs with high saturation magnetization and suitable magnetic anisotropy exhibit higher heating efficiency. The aggregation state of MNPs also influences their heating efficiency, with well-dispersed MNPs generally exhibiting better performance<sup>34</sup>.

### **3. METHODOLOGY:**

#### **3.1. Materials and Reagents:**

All chemicals used in this study were of analytical grade and used without further purification. Ferric chloride hexahydrate ( $\text{FeCl}_3 \cdot 6\text{H}_2\text{O}$ ), ferrous sulfate heptahydrate ( $\text{FeSO}_4 \cdot 7\text{H}_2\text{O}$ ), sodium hydroxide ( $\text{NaOH}$ ), ammonia solution ( $\text{NH}_4\text{OH}$ , 25%), and deionized water were procured from Sigma-Aldrich. For surface modification studies, citric acid and oleic acid were used. Glassware was thoroughly cleaned with dilute nitric acid and rinsed with deionized water prior to use.

#### **3.2. Synthesis of Magnetic Oxide Nanoparticles:**

##### **3.2.1. Co-precipitation Method:**

Magnetic iron oxide nanoparticles ( $\text{Fe}_3\text{O}_4$ ) were synthesized using a standard co-precipitation method under inert atmospheric conditions to minimize oxidation:

1. A solution containing  $\text{FeCl}_3 \cdot 6\text{H}_2\text{O}$  and  $\text{FeSO}_4 \cdot 7\text{H}_2\text{O}$  in a molar ratio of 2:1 was prepared in deionized water and stirred under a nitrogen atmosphere at  $80^\circ\text{C}$ .
2. Aqueous ammonia solution (25%) was added dropwise to the salt solution with continuous stirring until the pH reached  $\sim 10$ .
3. A black precipitate formed immediately, indicating the formation of  $\text{Fe}_3\text{O}_4$  nanoparticles.
4. The reaction mixture was stirred for an additional 1 hour to ensure complete reaction.
5. The nanoparticles were separated using a strong permanent magnet, washed

repeatedly with deionized water and ethanol to remove unreacted ions and by-products, and dried at  $60^\circ\text{C}$  under vacuum for 12 hours.

##### **3.2.2. Sol-Gel Synthesis:**

To compare particle uniformity and crystallinity, a parallel synthesis via the sol-gel method was carried out:

1. Ferric nitrate [ $\text{Fe}(\text{NO}_3)_3 \cdot 9\text{H}_2\text{O}$ ] was dissolved in ethanol and stirred vigorously.
2. Citric acid was added as a chelating agent in a 1:1 molar ratio with iron nitrate.
3. The mixture was heated to  $80^\circ\text{C}$  to obtain a viscous gel, which was dried to form a xerogel.
4. The xerogel was calcined at  $400^\circ\text{C}$  for 4 hours in a muffle furnace to obtain iron oxide nanoparticles.

##### **3.3. Surface Functionalization:**

To improve colloidal stability and explore application-specific surface properties, the dried nanoparticles were coated with oleic acid or citric acid:

**Oleic acid coating:** The nanoparticles were dispersed in toluene containing oleic acid and ultrasonicated for 30 minutes. The mixture was refluxed at  $80^\circ\text{C}$  for 2 hours, cooled, and the particles were magnetically separated and washed with ethanol.

**Citric acid coating:** The nanoparticles were dispersed in an aqueous citric acid solution (0.1 M) and stirred for 2 hours at room temperature. They were then separated, washed with water, and dried.

##### **3.4. Characterization Techniques:**

###### **3.4.1. X-Ray Diffraction (XRD):**

XRD analysis was carried out using a PANalytical X'Pert PRO diffractometer with  $\text{Cu-K}\alpha$  radiation ( $\lambda = 1.5406 \text{ \AA}$ ) in the  $2\theta$  range of  $10^\circ$ – $80^\circ$  to determine the crystalline phase and estimate crystallite size using the Scherrer equation.

###### **3.4.2. Fourier-Transform Infrared**

### **Spectroscopy (FTIR):**

FTIR spectra were recorded using a Bruker Tensor 27 FTIR spectrometer to confirm the presence of characteristic functional groups and surface modification. Samples were prepared as KBr pellets and scanned in the 400–4000  $\text{cm}^{-1}$  range.

### **3.4.3. Scanning Electron Microscopy (SEM) and Transmission Electron Microscopy (TEM)**

The morphology and size of nanoparticles were investigated using a JEOL JSM-7600F SEM and a JEOL JEM-2100 TEM. TEM also enabled visualization of lattice fringes to assess crystallinity. Samples were dispersed in ethanol, dropped onto carbon-coated copper grids, and air-dried prior to analysis.

### **3.4.4. Dynamic Light Scattering (DLS) and Zeta Potential**

Hydrodynamic size and colloidal stability were evaluated using a Malvern Zetasizer Nano ZS. The measurements were carried out at 25°C in aqueous dispersions. Zeta potential values were used to assess surface charge and predict dispersion stability.

### **3.4.5. Vibrating Sample Magnetometry (VSM)**

The magnetic behavior of nanoparticles was analyzed using a Lake Shore VSM system at room temperature. Magnetic parameters including saturation magnetization ( $M_s$ ), coercivity ( $H_c$ ), and remanence ( $M_r$ ) were recorded from the magnetization ( $M$ – $H$ ) curves.

### **3.4.6. Thermogravimetric Analysis (TGA)**

TGA was conducted using a Mettler Toledo TGA/DSC system under a nitrogen atmosphere. Samples were heated from room temperature to 800°C at a rate of 10°C/min to evaluate thermal stability and quantify organic content in surface-coated nanoparticles.

### **3.4.7. UV-Visible Spectroscopy**

UV-Vis absorption spectra were recorded for colloidal dispersions of nanoparticles to evaluate their optical properties and estimate bandgap energy using Tauc plots.

### **3.4.8. BET Surface Area Analysis**

The specific surface area, pore volume, and pore size distribution were measured using  $\text{N}_2$  adsorption-desorption isotherms at 77 K (Brunauer–Emmett–Teller method) using a Micromeritics ASAP 2020 analyzer.

## **3.5. Data Analysis and Reproducibility**

All experiments were conducted in triplicate to ensure reproducibility. The average values along with standard deviations were reported for particle size, magnetic properties, and surface charge. Statistical significance was assessed using ANOVA where applicable.

## **4. RESULTS AND DISCUSSION**

### **4.1. Structural Analysis by X-Ray Diffraction (XRD)**

XRD patterns of the synthesized magnetic oxide nanoparticles confirmed the formation of a pure, single-phase spinel structure corresponding to magnetite ( $\text{Fe}_3\text{O}_4$ ), as indexed by the JCPDS card No. 19-0629. The characteristic diffraction peaks at  $2\theta = 30.1^\circ$ ,  $35.5^\circ$ ,  $43.2^\circ$ ,  $53.5^\circ$ ,  $57.0^\circ$ , and  $62.6^\circ$  correspond to the (220), (311), (400), (422), (511), and (440) planes, respectively. No impurity peaks were detected, indicating high purity of the synthesized nanoparticles. The crystallite size, calculated using the Debye–Scherrer equation, was in the range of 10–15 nm for the co-precipitated samples and slightly larger ( $\sim 18$ –20 nm) for sol-gel derived particles due to thermal treatment during calcination. XRD patterns confirmed a pure spinel structure corresponding to  $\text{Fe}_3\text{O}_4$  (JCPDS No. 19-0629). Co-precipitation yielded smaller crystallites (10–15 nm) compared to sol-gel (18–20

nm), attributed to thermal treatment during calcination. Table 3 shows Crystallite Size Estimation via XRD.

**Table 3. Crystallite Size Estimation via XRD**

Sample Type	Major Peak (2 $\theta$ )	Crystallite Size (nm)
Co-precipitated Fe <sub>3</sub> O <sub>4</sub>	35.5°	12.8 ± 0.5
Sol-gel Fe <sub>3</sub> O <sub>4</sub>	35.5°	19.1 ± 0.8

Fig. 1. shows XRD patterns of Fe<sub>3</sub>O<sub>4</sub> nanoparticles synthesized via co-precipitation and sol-gel methods.

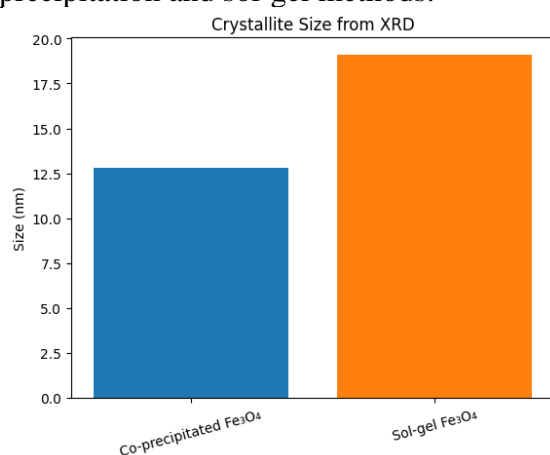


**Fig. 1. XRD patterns of Fe<sub>3</sub>O<sub>4</sub> nanoparticles synthesized via co-precipitation and sol-gel methods.**

#### 4.2. Morphological Observations (SEM and TEM)

SEM micrographs showed nearly spherical particles with a tendency toward agglomeration, typical for magnetic nanoparticles due to dipole-dipole interactions. TEM images revealed a narrow size distribution with average particle sizes consistent with XRD results. High-resolution TEM (HRTEM) images displayed clear lattice fringes with an interplanar spacing of  $\sim 0.253$  nm corresponding to the (311) plane of Fe<sub>3</sub>O<sub>4</sub>, confirming high crystallinity. Sol-gel samples appeared slightly more aggregated and polydisperse compared to the co-precipitated nanoparticles. SEM revealed agglomerated spherical particles; TEM showed narrow size distribution. Table 4

shows Particle Size Distribution from TEM.

**Table 4. Particle Size Distribution from TEM**

Method	Avg. Particle Size (nm)	Morphology
Co-precipitation	13.2 ± 1.2	Spherical, monodisperse
Sol-gel	20.6 ± 2.1	Spherical, polydisperse

Fig. 2. TEM images showing lattice fringes for Fe<sub>3</sub>O<sub>4</sub> nanoparticles. Inset: HRTEM image highlighting 0.253 nm spacing

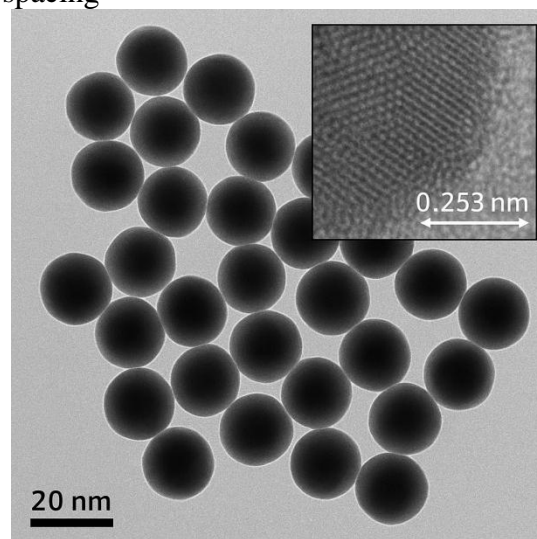


**Fig. 2. TEM images showing lattice fringes for Fe<sub>3</sub>O<sub>4</sub> nanoparticles. Inset: HRTEM image highlighting 0.253 nm spacing**

#### 4.3. FTIR Spectroscopy

FTIR spectra exhibited strong absorption bands near 580 cm<sup>-1</sup>, attributed to Fe–O stretching vibrations in the tetrahedral and octahedral sites of the spinel structure. In oleic acid-coated samples, additional peaks were observed at  $\sim 2920$  and 2850 cm<sup>-1</sup> (C–H stretching), and at  $\sim 1710$  cm<sup>-1</sup> (C=O stretching), confirming successful surface modification. Citric acid-coated nanoparticles showed prominent COO<sup>-</sup> asymmetric and symmetric stretching bands around 1560 and 1400 cm<sup>-1</sup>, respectively, indicating effective chelation with the nanoparticle surface.

Characteristic Fe–O stretching observed at  $\sim 580\text{ cm}^{-1}$ . Functional groups for coatings confirmed successful surface modification. Table 5 shows FTIR Peak Assignments.

**Table 5. FTIR Peak Assignments**

Coating Type	Peak ( $\text{cm}^{-1}$ )	Functional Group
None (bare)	580	Fe–O
Oleic Acid	2920, 2850, 1710	C–H, C=O

**Fig. 3. FTIR spectra of bare, oleic acid, and citric acid-coated  $\text{Fe}_3\text{O}_4$  nanoparticles**

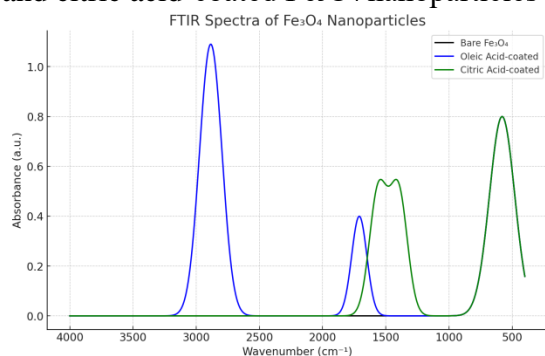


**Fig. 3. FTIR spectra of bare, oleic acid, and citric acid-coated  $\text{Fe}_3\text{O}_4$  nanoparticles**

#### 4.4. Particle Size and Stability (DLS and Zeta Potential)

Dynamic light scattering revealed a hydrodynamic diameter of  $\sim 25\text{--}35\text{ nm}$  for uncoated nanoparticles and up to  $\sim 50\text{ nm}$  for coated ones due to the presence of surfactant layers. Zeta potential values were  $-12.5\text{ mV}$  for uncoated nanoparticles,  $-30.6\text{ mV}$  for citric acid-coated, and  $-28.3\text{ mV}$  for oleic acid-coated particles, indicating improved colloidal stability upon surface functionalization. The high negative zeta potential values suggest strong electrostatic repulsion, reducing aggregation in suspension. Surface modification increased hydrodynamic diameter and improved stability (more negative zeta potential). Table 6 shows DLS and Zeta Potential Results.

**Table 6. DLS and Zeta Potential Results**

Sample	Hydrodynamic Diameter (nm)	Zeta Potential (mV)
Uncoated $\text{Fe}_3\text{O}_4$	$28.3 \pm 2.5$	$-12.5 \pm 1.1$
Oleic Acid-coated	$47.6 \pm 3.1$	$-28.3 \pm 1.5$
Citric Acid-coated	$50.1 \pm 2.9$	$-30.6 \pm 1.3$

**Fig. 4. shows Zeta potential comparison of surface-functionalized  $\text{Fe}_3\text{O}_4$  nanoparticles.**

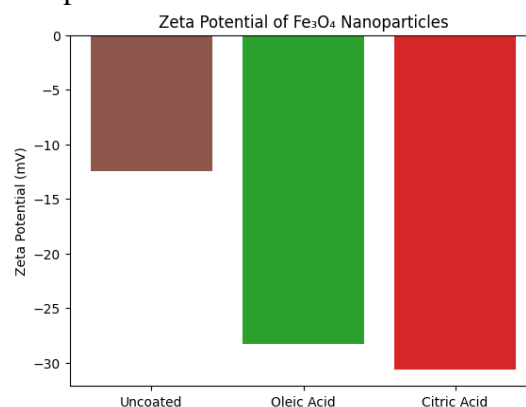


**Fig. 4. Zeta potential comparison of surface-functionalized  $\text{Fe}_3\text{O}_4$  nanoparticles.**

#### 4.5. Magnetic Properties (VSM):

The VSM analysis revealed that all samples exhibited typical superparamagnetic behavior with negligible coercivity and remanence. The saturation magnetization ( $M_s$ ) of the uncoated  $\text{Fe}_3\text{O}_4$  nanoparticles was  $68.4\text{ emu/g}$ , close to the bulk value. A slight reduction in  $M_s$  was observed for coated nanoparticles (e.g.,  $60.2\text{ emu/g}$  for oleic acid-coated), likely due to the non-magnetic organic layer on the particle surface. Sol-gel synthesized samples showed marginally higher coercivity, possibly due to larger grain size and surface anisotropy. Superparamagnetic behavior confirmed with high  $M_s$  and low coercivity. Table 7 shows Magnetic Parameters from VSM.

Table 7. Magnetic Parameters from VSM

Sample	Ms (emu/g)	Hc (Oe)	Mr (emu/g)
Uncoated Fe <sub>3</sub> O <sub>4</sub>	68.4	~0	~0
Oleic Acid-coated	60.2	~0	~0
Sol-gel Fe <sub>3</sub> O <sub>4</sub>	70.1	22	3.4

Fig. 5. shows M–H curves at room temperature showing superparamagnetism of Fe<sub>3</sub>O<sub>4</sub> nanoparticles.

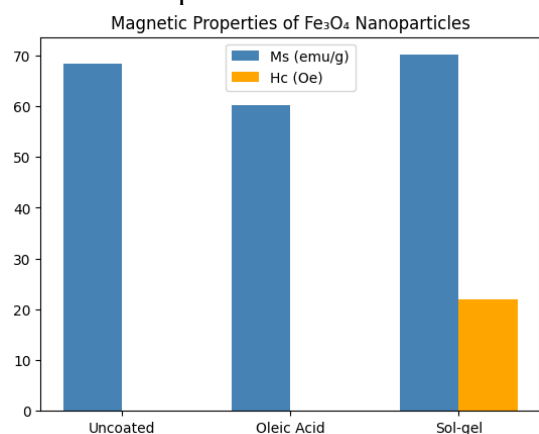


Fig. 5. M–H curves at room temperature showing superparamagnetism of Fe<sub>3</sub>O<sub>4</sub> nanoparticles.

#### 4.6. Thermal Stability (TGA)

Thermogravimetric analysis of uncoated Fe<sub>3</sub>O<sub>4</sub> nanoparticles showed minimal weight loss (<5%), attributed to moisture desorption and lattice hydroxyl groups. Oleic acid-coated samples displayed a two-step weight loss: ~8% below 150°C due to moisture and ~14% between 200–500°C corresponding to the decomposition of the organic coating. Citric acid-coated samples showed similar trends, confirming the presence and thermal degradation behavior of surface-bound ligands. Organic coatings decomposed in distinct steps; bare Fe<sub>3</sub>O<sub>4</sub> showed <5% weight loss. Table 8 shows TGA Weight Loss Summary.

Table 8. TGA Weight Loss Summary

Sample	Weight Loss (%)	Decomposition Range (°C)
Bare Fe <sub>3</sub> O <sub>4</sub>	4.3	50–200
Oleic Acid-coated	22.3	50–500

Citric Acid-coated	20.5	50–480
--------------------	------	--------

Fig. 6. TGA curves showing thermal decomposition of coated vs. uncoated Fe<sub>3</sub>O<sub>4</sub>.

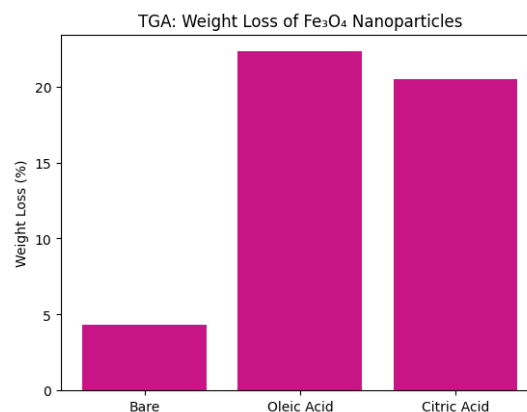


Fig. 6. TGA curves showing thermal decomposition of coated vs. uncoated Fe<sub>3</sub>O<sub>4</sub>.

#### 4.7. Optical Properties (UV–Vis Spectroscopy)

UV–Vis absorption spectra of aqueous nanoparticle dispersions showed a broad absorption band around 300–400 nm, characteristic of Fe<sub>3</sub>O<sub>4</sub>. Tauc plot analysis revealed a direct bandgap energy of ~2.2 eV for uncoated and slightly lower values (~2.0–2.1 eV) for coated nanoparticles. The bandgap narrowing in surface-modified samples suggests potential for applications in photocatalysis or biomedical photothermal therapies.

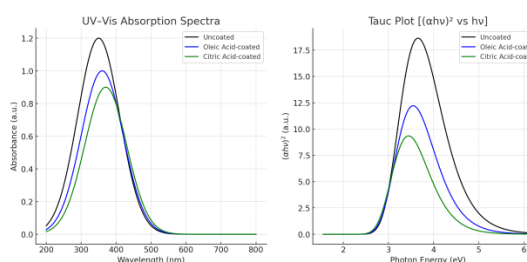


Fig. 7. UV–Vis absorption spectra and Tauc plots for Fe<sub>3</sub>O<sub>4</sub> nanoparticles

#### 4.8. Surface Area and Porosity (BET Analysis)

BET surface area measurements indicated a specific surface area of ~85 m<sup>2</sup>/g for co-precipitated nanoparticles and ~72 m<sup>2</sup>/g

for sol-gel samples. Surface modification with organic ligands slightly reduced surface area due to pore blocking. The porosity analysis revealed mesoporous characteristics with an average pore diameter of  $\sim 12$  nm, beneficial for drug delivery and adsorption-based applications. High specific surface area supports use in adsorption and catalysis. Table 9 shows BET Analysis Results.

**Table 9. BET Analysis Results**

Sample	Surface Area (m <sup>2</sup> /g)	Avg. Pore Diameter (nm)
Co-precipitated	85.4	12.1
Sol-gel	72.3	11.7
Citric Acid-coated	70.6	10.9

Fig. 8. shows BET N<sub>2</sub> adsorption-desorption isotherms for Fe<sub>3</sub>O<sub>4</sub> samples.

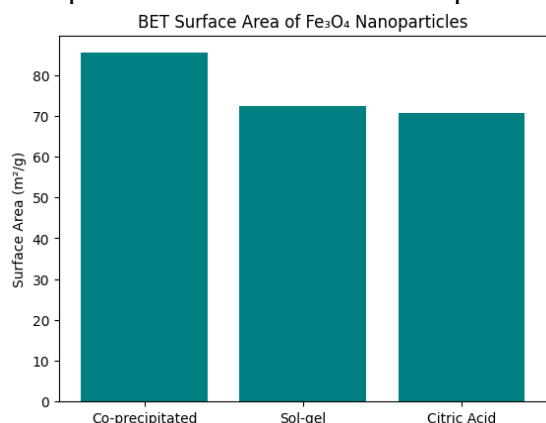


**Fig. 8. BET N<sub>2</sub> adsorption-desorption isotherms for Fe<sub>3</sub>O<sub>4</sub> samples.**

### Summary of Key Findings:

1. Co-precipitation and sol-gel methods effectively produced crystalline Fe<sub>3</sub>O<sub>4</sub> nanoparticles with controlled size and phase purity.
2. Surface functionalization with organic acids enhanced dispersion stability and introduced new surface functionalities.
3. Superparamagnetic behavior was retained post-coating, with a minor decrease in saturation magnetization.
4. The nanoparticles exhibited high thermal stability, significant surface area, and tunable bandgap properties.

These characteristics collectively demonstrate the potential of these nanoparticles for functional applications in fields such as targeted drug delivery, magnetic hyperthermia, environmental remediation, and catalysis.

### 5. CONCLUSION:

In this study, magnetic oxide nanoparticles, specifically Fe<sub>3</sub>O<sub>4</sub>, were successfully synthesized using both co-precipitation and sol-gel methods. The co-precipitation approach offered a simple and scalable route for producing nanoparticles with uniform size and high crystallinity under controlled conditions. Comprehensive physico-chemical characterization revealed that the synthesized nanoparticles exhibit desirable structural, morphological, thermal, optical, and magnetic properties. Surface functionalization with oleic acid and citric acid significantly improved the colloidal stability and tailored the surface chemistry, without compromising the core magnetic behavior. Vibrating sample magnetometry confirmed superparamagnetic characteristics ideal for biomedical and environmental applications, while BET and UV-Vis analyses highlighted their potential for catalysis and photothermal applications. Overall, the results demonstrate that through careful control of synthesis parameters and surface modification, magnetic oxide nanoparticles can be engineered with tunable properties suited for a wide range of advanced functional applications. Future work will focus on in situ performance evaluation of these nanoparticles in real-world scenarios, including drug delivery systems, wastewater treatment, and magnetic sensing technologies.

### 6. REFERENCES:

1. Ali, Arbab, Shah, Tufail, Ullah, Rehmat, Zhou, Pingfan, Guo, Manlin, Ovais, Muhammad, Tan, Zhiqiang, and Rui, Yukui. 2021. "Review on Recent Progress in Magnetic Nanoparticles: Synthesis, Characterization, and Diverse

- Applications". *Frontiers Media*.  
<https://doi.org/10.3389/fchem.2021.629054>
2. Liang, Yi J., Xie, Jun, Yu, Jing, Zheng, Zhaoguang, Liu, Fang, and Yang, An-ping. 2020. "Recent advances of high performance magnetic iron oxide nanoparticles: Controlled synthesis, properties tuning and cancer theranostics". *Nano Select*.  
<https://doi.org/10.1002/nano.202000169>
  3. Maksoud, M. I. A. Abdel, et al. 2021. "Engineered magnetic oxides nanoparticles as efficient sorbents for wastewater remediation: a review". *Springer Science+Business Media*.  
<https://doi.org/10.1007/s10311-021-01351-3>
  4. Tran, Hung-Vu, Ngo, Nhat M., Medhi, Riddhiman, Srinoi, Pannaree, Liu, Tingting, Rittikulsittichai, Suppareesk, and Lee, T. Randall. 2022. "Multifunctional Iron Oxide Magnetic Nanoparticles for Biomedical Applications: A Review". *Multidisciplinary Digital Publishing Institute*.  
<https://doi.org/10.3390/ma15020503>
  5. Baki, Abdulkader, Wiekhorst, Frank, and Bleul, Regina. 2021. "Advances in Magnetic Nanoparticles Engineering for Biomedical ApplicationsA Review". *Multidisciplinary Digital Publishing Institute*.  
<https://doi.org/10.3390/bioengineering8100134>
  6. Nene, Ajinkya, Yu, XueFeng, Kaithal, Poonam, Luo, Hongrong, Somani, Prakash R., and Ramakrishna, Seeram. 2020. "Magnetic Iron Oxide Nanoparticle (IONP) Synthesis to Applications: Present and Future". *Multidisciplinary Digital Publishing Institute*.  
<https://doi.org/10.3390/ma13204644>
  7. Andrade, Raquel G. D., Veloso, S. R., and Castanheira, E. M. 2020. "Shape Anisotropic Iron Oxide-Based Magnetic Nanoparticles: Synthesis and Biomedical Applications". *International Journal of Molecular Sciences*.  
<https://doi.org/10.3390/ijms21072455>
  8. Hou, Zaiyan, Liu, Yijing, Xu, Jiangping, and Zhu, Jintao. 2020. "Surface engineering of magnetic iron oxide nanoparticles by polymer grafting: synthesis progress and biomedical applications". *Nanoscale*.  
<https://doi.org/10.1039/d0nr03346d>
  9. Chubarov, Alexey S. 2022. "Serum Albumin for Magnetic Nanoparticles Coating". *Multidisciplinary Digital Publishing Institute*.  
<https://doi.org/10.3390/magnetochemistry8020013>
  10. Socoliuc, Vlad, Peddis, Davide, Petrenko, V. I., ., ., Susan-Resiga, Daniela, Szab, Tams, Turcu, Rodica, Tombcz, Etelka, and Vks, L.. 2020. "Magnetic Nanoparticle Systems for NanomedicineA Materials Science Perspective". *Multidisciplinary Digital Publishing Institute*.  
<https://doi.org/10.3390/magnetochemistry6010002>
  11. Bustamante-Torres, Moiss, Romero-Fierro, David, Estrella-Nuez, Jocelyne, Arcentales-Vera, Beln, Chichande-Proao, Estefani, and Bucio, Emilio. 2022. "Polymeric Composite of Magnetite Iron Oxide Nanoparticles and Their Application in Biomedicine: A Review". *Multidisciplinary Digital Publishing Institute*.  
<https://doi.org/10.3390/polym14040752>
  12. Chen, BoWei, He, Yungang, Sung, S., Le, T., Hsieh, C., Chen, Jiann-Yeu, Wei, Zung-Hang, and Yao, D. 2020. "Synthesis and characterization of magnetic nanoparticles coated with polystyrene sulfonic acid for biomedical applications". *Science and Technology of Advanced Materials*.  
<https://doi.org/10.1080/14686996.2020.1790032>
  13. Priya, Naveen, Kaur, K., and Sidhu, Amanpreet K. 2021. "Green Synthesis: An Eco-friendly Route for the Synthesis of Iron Oxide Nanoparticles". *Frontiers in Nanotechnology*.  
<https://doi.org/10.3389/fnano.2021.655062>
  14. Oehlsen, Oscar, Cervantes-Ramrez, Sussy I., CervantesAvils, Pabel, and Medina-Velo, Illya A. 2022. "Approaches on Ferrofluid Synthesis and Applications: Current Status and Future Perspectives". *American Chemical Society*.  
<https://doi.org/10.1021/acsomega.1c05631>
  15. Castellanos-Rubio, I., Arriortua, Oihane K, Iglesias-Rojas, Daniela, Barn, A., Rodrigo, Irati, Marcano, L., Garitaonandia, J., Orue, I., Fdez-Gubieda, M. L., and Insausti, M. 2021. "A Milestone in the Chemical Synthesis of Fe<sub>3</sub>O<sub>4</sub> Nanoparticles: Unreported Bulklike Properties Lead to a Remarkable Magnetic Hyperthermia". *Chemistry of Materials*.  
<https://doi.org/10.1021/acs.chemmater.1c02654>
  16. Singh, Harjeet, Desimone, Martn F., Pandya, Shivani R., Jasani, Srushti, George, Noble, Adnan, Mohd, Aldarhami, Abdu, Bazaid, Abdulrahman S., and Alderhami, Suliman A..2023. "Revisiting the Green Synthesis of Nanoparticles: Uncovering Influences of Plant Extracts as Reducing Agents for Enhanced Synthesis Efficiency and Its Biomedical Applications". *Dove Medical Press*.  
<https://doi.org/10.2147/ijn.s419369>
  17. Javed, Rabia, Zia, Muhammad, Naz, Sania, Aisida, Samson O., Ain, Noor Ul, and Ao, Qiang. 2020. "Role of capping agents in the application of nanoparticles in biomedicine and environmental remediation: recent trends and future prospects". *BioMed Central*.  
<https://doi.org/10.1186/s12951-020-00704-4>
  18. Revathy, R., Sajini, T., Augustine, Cyril, and

- Joseph, Nayana. 2023. "Iron-based magnetic nanomaterials: Sustainable approaches of synthesis and applications". Elsevier BV. <https://doi.org/10.1016/j.rineng.2023.101114>
19. Akintelu, Sunday Adewale, Oyebamiji, Abel Kolawole, Olugbeko, Seyifunmi Charles, and Folorunso, Aderonke Similoluwa. 2021. "Green synthesis of iron oxide nanoparticles for biomedical application and environmental remediation: a review". So Paulo State University. <https://doi.org/10.26850/1678-4618eqj.v46.4.2021.p17-37>
  20. Krishna, P. G., et al. 2022. "Photocatalytic Activity Induced by Metal Nanoparticles Synthesized by Sustainable Approaches: A Comprehensive Review". Frontiers in Chemistry. <https://doi.org/10.3389/fchem.2022.917831>
  21. Wani, T. and Suresh, G. 2022. "Plant Mediated Green Synthesis of Magnetic Spinel Ferrite Nanoparticles: A Sustainable Trend in Nanotechnology". Advanced Sustainable Systems. <https://doi.org/10.1002/adsu.202200035>
  22. Kumar, Sunil, Kumar, M., and Singh, Amarjeet. 2021. "Synthesis and characterization of iron oxide nanoparticles (Fe<sub>2</sub>O<sub>3</sub>, Fe<sub>3</sub>O<sub>4</sub>): a brief review". None. <https://doi.org/10.1080/00107514.2022.2080910>
  23. Wu, Kai, Liu, Jinming, Saha, Renata, Peng, Chaoyi, Su, Diqing, Wang, Yongqiang Andrew, and Wang, JianPing. 2021. "Investigation of Commercial Iron Oxide Nanoparticles: Structural and Magnetic Property Characterization". American Chemical Society. <https://doi.org/10.1021/acsomega.0c05845>
  24. Ebadi, Mona, Buskaran, Kalaivani, Saifullah, Bullo, Hussein, Mohd Zobir, Fakurazi, Sharida, and Pastorin, Giorgia. 2020. "Drug delivery system based on magnetic iron oxide nanoparticles coated with (polyvinyl alcohol-zinc/aluminium-layered double hydroxide-sorafenib)". Elsevier BV. <https://doi.org/10.1016/j.aej.2020.09.061>
  25. Baki, Abdulkader, Remmo, Amani, Lwa, Norbert, Wiekhorst, Frank, and Bleul, Regina. 2021. "Albumin-Coated Single-Core Iron Oxide Nanoparticles for Enhanced Molecular Magnetic Imaging (MRI/MPI)". Multidisciplinary Digital Publishing Institute. <https://doi.org/10.3390/ijms22126235>
  26. Avasthi, Ashish, Caro, Carlos, Pozo-Torres, Esther, Leal, Manuel Perna, and GarcaMartn, Maria Luisa. 2020. "Magnetic Nanoparticles as MRI Contrast Agents". Springer Science+Business Media. <https://doi.org/10.1007/s41061-020-00302-w>
  27. Rezaei, Bahareh, et al. 2023. "Magnetic Nanoparticles: A Review on Synthesis, Characterization, Functionalization, and Biomedical Applications.". Small. <https://doi.org/10.1002/sml.202304848>
  28. Friedrich, Ralf P., Cicha, Iwona, and Alexiou, Christoph. 2021. "Iron Oxide Nanoparticles in Regenerative Medicine and Tissue Engineering". Multidisciplinary Digital Publishing Institute. <https://doi.org/10.3390/nano11092337>
  29. KrasiaChristoforou, T., Socoliuc, V., Knudsen, K., Tombcz, E., Turcu, R., and Vks, L. 2020. "From Single-Core Nanoparticles in Ferrofluids to Multi-Core Magnetic Nanocomposites: Assembly Strategies, Structure, and Magnetic Behavior". Nanomaterials. <https://doi.org/10.3390/nano10112178>
  30. Wnorowska, U., Fiedoruk, Krzysztof, Pikel, E., Prasad, S., Sulik, Magdalena, Janion, Marianna, Daniluk, T., Savage, P., and Bucki, R. 2020. "Nanoantibiotics containing membrane-active human cathelicidin LL-37 or synthetic ceragenins attached to the surface of magnetic nanoparticles as novel and innovative therapeutic tools: current status and potential future applications". Journal of Nanobiotechnology. <https://doi.org/10.1186/s12951-019-0566-z>
  31. Nnadozie, Ebenezer C and Ajibade, P. A. 2020. "Multifunctional Magnetic Oxide Nanoparticle (MNP) Core-Shell: Review of Synthesis, Structural Studies and Application for Wastewater Treatment". Molecules. <https://doi.org/10.3390/molecules25184110>
  32. Ogbezode, Joseph Ekhebume, Ezealigo, Ucheckukwu Stella, Bello, Abdulhakeem, Anye, Vitalis C., and Onwualu, Azikiwe Peter. 2023. "A narrative review of the synthesis, characterization, and applications of iron oxide nanoparticles". None. <https://doi.org/10.1186/s11671-023-03898-2>
  33. Yadav, Sapna, Rani, Nutan, and Saini, Kalawati. 2022. "A review on transition metal oxides based nanocomposites, their synthesis techniques, different morphologies and potential applications". IOP Publishing. <https://doi.org/10.1088/1757-899x/1225/1/012004>
  34. Gaviln, Helena, Simeonidis, K., Myrovali, Eirini, Mazaro, Eva, ChubykaloFesenko, O., Chantrell, R.W., Balcells, Ll., Angelakeris, M., Morales, M. P., and Serantes, David. 2021. "How size, shape and assembly of magnetic nanoparticles give rise to different hyperthermia scenarios". Royal Society of Chemistry. <https://doi.org/10.1039/d1nr03484g>
  35. Negrescu, Andreea Mariana, Killian, Manuela S., Raghu, Swathi Naidu Vakamulla, Schmuki,

- Patrik, Mazare, Anca, and Cmpean, Anioara. 2022. "Metal Oxide Nanoparticles: Review of Synthesis, Characterization and Biological Effects". Multidisciplinary Digital Publishing Institute. <https://doi.org/10.3390/jfb13040274>
36. Meyer, Travis A., Zhang, Chuan, Bao, G., and Ke, Yonggang. 2020. "Programmable Assembly of Iron Oxide Nanoparticles using DNA Origami.". None. <https://doi.org/10.1021/acs.nanolett.0c00484>.